ACS OMEGA

http://pubs.acs.org/journal/acsodf

Article

A Sensor-Integrated Face Mask Using Au@SnO_2 Nanoparticle Modified Fibers and Augmented Reality Technology

Tzu-En Lin,* Ming-Chun Chien, Po-Feng Chen, Pei-Wen Yang, Huai-En Chang, Ding-Han Wang, Tung-Yi Lin, and Yung-Jung Hsu

Cite This: *ACS Omega* 2022, 7, 42233−42241

Read Online

ACCESS | Metrics & More | Article Recommendations | Supporting Information

ABSTRACT: In this work, we develop a wireless sensor-integrated face mask using Au@SnO_2 nanoparticle-modified conductive fibers based on augmented reality (AR) technology. AR technology enables the overlay of real objects and environments with virtual 3D objects and allows virtual interactions with real objects to create desired meanings. With the help of the AR system, the size of the mask could be precisely estimated and then manufactured using 3D printing technology. The body temperature sensor and respiratory sensor were integrated into the mask so that vital parameters of the human body could be continuously monitored without removing the personal protective equipment. Furthermore, the outer part of the mask consists of conductive fabric modified with Au@SnO_2 core−shell nanoparticle additives, which enhanced the filtration efficiency of airborne aerosols. A significant improvement in the filtration efficiency of particulate matter 2.5 was observed after applying an external voltage to the conductive textiles. A smartwatch with a heart rate sensor was paired with the mask to display sensor data on the mask through wireless transmission. Therefore, this sensor-integrated mask system with AR technology provides the first line of defense to combat global threats from pathogens and air pollutants.

1. INTRODUCTION

The coronavirus (COVID-19) pandemic imposed extraordinary requirements on the health system, resulting in higher risks of infections associated with the health system (HAI).[1,2] Unfortunately, the burden of personal protective equipment (PPE), such as face masks, eyewear, and isolation gowns, restricts real-time monitoring of body temperature, respiratory rate, and other vital parameters. Therefore, developing a biosensor-integrated face mask could reduce the risk of infections associated with the health system because front-line clinicians do not need to remove the PPE to measure vital signs.

To address the above-mentioned problem and improve the safety of healthcare workers, various smart masks and smart textiles have recently been developed.[3−7] Other types of functional masks have been reported in the literature, including masks with self-sterilizable air filters,[8] masks with dry heat sterilization,[9] and a machine learning variable pore mask.[10] However, they usually have limited functions or can only detect a certain target analyte.[11−14] Furthermore, the size and shape of these advanced masks could not be easily adjusted according to the user. In general, a 3D scanner and other complex instruments are required to obtain the features of the human face to make custom masks.[15] To overcome this problem, the architecture of the face mask was personalized in augmented reality (AR) for adults and children in this research.[16,17] Different ratios of the human skull and the thickness of the buccal fat were considered at different ages. Virtual head models enable the simulation of mask adaptation in adults or children in the mobile AR system. Subsequently, the mask was manufactured using 3D printing technology.[18]

The sensor-integrated mask system consisted of two parts. The outer part was the conductive fabric modified with inorganic nanoparticle additives, a type of photocatalyst and charge enhancer that could generate free radicals to maintain a self-cleaning surface.[19−22] In this work, nontoxic Au@SnO_2 core−shell nanoparticles were used as a charge enhancer.[23,24] The reason is that the electrostatic interactions between fine particles and conductive fabric can be improved if Au@SnO_2 is used as an electret.[25,26] Since most dust particles (e.g., particulate matter 2.5, PM 2.5) and microbes are electrostatically charged[27,28] and can be attracted by conductive fabric if a voltage is applied to it.[29−32] This improvement can be further enhanced under biased external conditions, leading to higher filtration efficiency in PM2.5.

Received: August 8, 2022
Accepted: October 11, 2022
Published: November 11, 2022

https://doi.org/10.1021/acsomega.2c04655
ACS Omega 2022, 7, 42233−42241

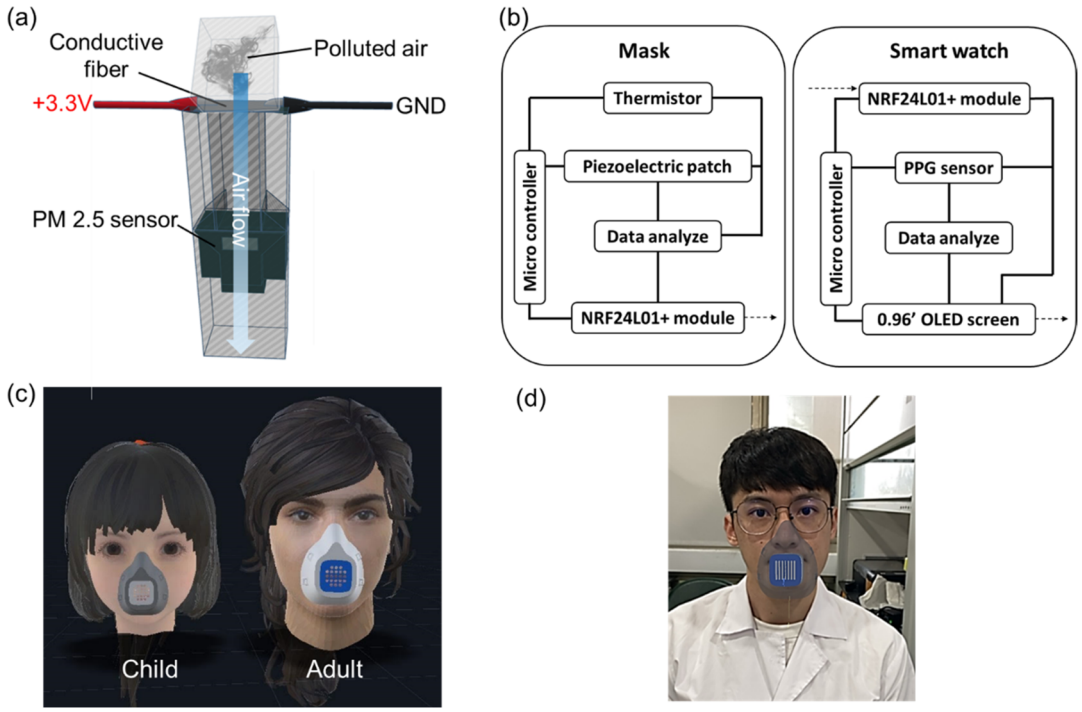

Figure 1. (a) Schematic representation of the device and the PM 2.5 sensor designed to measure the filtration efficiency of the conductive fabric. (b) Flowchart of the sensing part of the intelligent mask. Integration of sensor measurements into the mask and wireless synchronization of them with the smartwatch. (c) Virtual simulation of masks worn by a child and an adult. (d) Preview of the mask-wearing on a male face in AR.

The inner part of the mask consisted of an electronic microcontroller with two sensors, a temperature sensor and a respiratory sensor to monitor body temperature and respiratory rate. The microcontroller then integrated and wirelessly transmitted the data to the smartwatch. In conjunction with the photoplethysmography (PPG) sensor on the smartwatch, the vital parameters information could be collected at one time and displayed through the organic light-emitting diode (OLED) displayer on the smartwatch. PPG is a noninvasive technology that measures blood flow volume using an optical source and a photodetector on the skin surface.[33] Therefore, the intelligent mask not only improved protection by using conductive fabrics and nanoparticles but also integrated various sensor systems for real-time sensing without removing the mask.

2. MATERIALS AND METHODS

2.1. Chemicals. Gold chloride ($HAuCl_4{\cdot}3H_2O$, 99.9%), sodium stannate ($Na_2Sn_2O_3{\cdot}3H_2O$, 95%), Nafion, isopropyl alcohol (IPA), and trisodium citrate ($C_6H_5Na_3O_7{\cdot}2H_2O$, 99%) were purchased from Sigma-Aldrich. The conducting fabrics were purchased from Composite Hybrid International Co., Ltd. The DN7C3CA007 IR dust sensor (PM 2.5 sensor) was purchased from Sharp, Japan. The thermoplastic polyurethane (TPU) was from Ever 3D, Taiwan. The LM35DZ temperature sensor was purchased from Texas Instruments, USA.

2.2. Synthesis and Characterization of Au@SnO_2 Core–Shell Nanoparticles. The suspension of Au nanoparticles with an average particle diameter of 15 nm was first prepared using a citrate reduction method according to the previous report.[25] The SnO_2 layer on the Au nanoparticles was then carried out using a chemical precipitation method.[34] 5 mL of $Na_2Sn_2O_3$ solution (40 mM) was added to 150 mL of Au nanoparticle suspension. The mixed solution was stirred at 75 °C for 20 min and then naturally cooled to room temperature. Subsequently, the reaction solution was centrifuged and washed 3 times with deionized water to collect the Au@SnO_2 core–shell nanoparticles. Scanning electron microscopy (SEM) images were taken with a Hitachi SU-8010 microscope. Transmission electron microscopy (TEM) images were taken with a JEOL JEM-F200 microscope. X-ray diffraction (XRD) patterns were recorded on a Bruker D2 PHASER diffractometer.

2.3. Modification of Conductive Fabrics with Au@SnO_2 Nanoparticles. To improve PM 2.5 filtration efficiency, Au@SnO_2 nanoparticles were coated on the conductive fabrics.[35] The nanoparticles (5 mg) were first dispersed in a solution comprising 1 mL of IPA and 50 μL of Nafion. The conductive fabric was trimmed into a rectangle 2.5 cm in width and 2.5 cm in length. The Au@SnO_2 suspension was ultrasonicated for 10 min. Subsequently, the conductive fabric was soaked in suspension for 3 h. Subsequently, the modified conductive fabric was removed and heated to 50 °C until all its adsorbed liquids were dried. As shown in Figure S1-2 (SI-1, SEM images of Au@SnO_2 modified conductive fabric), the introduced Au@SnO_2 nanoparticles were integrated with the fiber bundles with the fiber surface covered with many Au@SnO_2.

2.4. Measurement of PM2.5 Particles. To measure the filtration efficiency of the conductive fabric, we designed a device with both ends open and a PM 2.5 sensor in the middle.[36] PM for testing were produced from burning incense.[37,38] Most PM generated by burning incense would pass through (or adsorbed on) the conductive fabric and then through the PM 2.5 sensor so that we could evaluate the ability to block PM 2.5 between the different conductive fabrics.[39,40] The design of the device hardware is shown in Figure 1a.

https://doi.org/10.1021/acsomega.2c04655
ACS Omega 2022, 7, 42233−42241

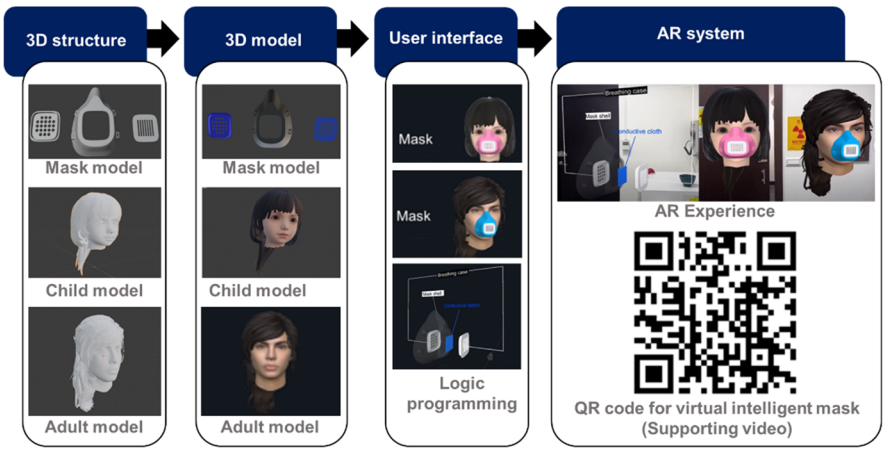

Figure 2. Workflow for building an AR system.

In the PM 2.5 sensor (DN7C3CA007 IR dust sensor), there was a pair of built-in infrared red (IR) emitters and receivers in this sensor. When air particles passed through the sensor, the fan screened PM 2.5, which had smaller inertia, and divided it into different channels to eliminate interference from other particles. Consequently, PM 2.5 particles scattered the IR light source generated by the IR emitter, thus attenuating the light that the IR receiver receives. After amplification, the signal was sent to Arduino for calculation, and we could obtain the PM 2.5 concentration by analyzing the different attenuating levels of the IR signal.[41]

2.5. Fabrication of the Smartwatch System. Figure 1b shows the design of the smartwatch paired with the mask. The smartwatch was built with the Max30102 heart rate sensor, microcontroller, and the NRF24L01+ wireless transmission module. The microcontroller received the data from the thermistor and respiratory sensor and then transmitted the signals through the wireless transmission module NRF24L01+.[42] Subsequently, the signals were integrated and displayed on the 0.96-in. OLED screen.

2.6. Wireless Transmission. Arduino pro mini, a tiny microcontroller, was used to integrate the temperature and respiratory sensors. After collecting and calculating, we sent the processed data to our smartwatch with the wireless transmission module NRF24L01+, which has 126 channels from 2.4 to 2.525 GHz, and each channel can accommodate up to six lines. Therefore, multi-to-one wireless communication can be achieved. Communication between transmitting and receiving modules can be carried out by establishing the same channel. In this study, we used a pair of transmission modules to send the processed data from our mask to the smartwatch. The flowchart for this is shown in Figure 1b, as mentioned above.

2.7. 3D Printing of the Face Mask. In this work, 'Tinkercad', an online software, was used to design and create 3D face masks and human models (adult and child). The 3D structure of the face mask was designed on the concept of a gas respirator. After finishing the scripts in Tinkercad, we saved them as STL files, and we could use these STL files to make AR models (Figure 1c,d). After adjusting and customizing the mask size in the AR system, we exported the final STL file to a 3D printer to build the mask architecture. In this study, thermoplastic polyurethane (TPU) was chosen as the mask architecture material, as it was flexible and durable, making it suitable for contacting the faces without scratching them.[43] The temperature sensor was installed in the face mask. Details of the calibration of the body temperature sensor and the optimization of the breathing rate sensor are provided in the Supporting Information (SI-2, The calibration of the body temperature sensor; SI-3 The optimization of the breathing rate sensor; SI-4 Collection of voltage signals caused by respiration; SI-5 Eliminating noise from body movement). The STL file was imported into a continuous filament writing 3D printer (INFINITY3DP NEW X1) to fabricate the face mask. After several tests, the face mask was successfully printed.

2.8. Preparation of the AR System. To import 3D models into the mobile XR system, the mobile XR app (RISAR, Mifly, Taiwan) was installed on a personal smartphone. The workflow to integrate 3D mask models into the AR system is shown in Figure 2. First, STL models were designed in Blender software using computer-aided design (CAD) technology, rendering those 3D models with proper colors. Second, STL models were converted to OBJ models and imported into the AR system. Next, logic programming was coded in the AR system, for model interactions, such as zoom and rotation, to each model. Finally, the scene was sent to the mobile XR app, and the user's smartphone demonstrates the AR. Note that a similar workflow could also be applied to other types of AR or VR headsets. From the QRcode, the mask models could be observed in the demonstration video. Taking into account the different ratios of the human skull and the thickness of the buccal fat at different ages, we also used digital head models of children and adults to present the customizability of the masks in the mobile AR system.

3. RESULTS AND DISCUSSION

3.1. Design and AR System of the Sensor-Integrated Mask. In the past, the traditional display of 3D structures with 2D images exposes many disadvantages, such as losing a lot of 3D structure information, difficulty showing customization capabilities, and hardly imagining the situation of people wearing masks. To apply complete 3D structural information, customization feasibility, and intuitive operation to simulate the appearance of wearing a mask, the exploded view of the sensor-integrated mask is shown in Figure 1c using mobile extended reality (XR) technology. Figure 1c shows the virtual faces of an adult and a child wearing the 3D printed sensor-integrated mask. The tightness of the masks was examined. The virtual simulation showed that if the child's mask was directly miniaturized from the adult's mask, there was an interspace between the face and the mask. Therefore, the shape

https://doi.org/10.1021/acsomega.2c04655
ACS Omega 2022, 7, 42233−42241

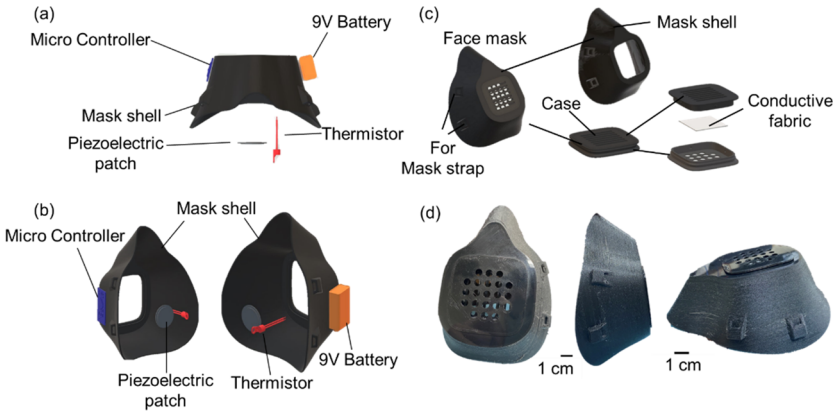

Figure 3. (a) Schematic representation of the structure of face masks (top view). (b) Schematic representation of the structure of the face masks (side view). (c) Mask shell structure and breathing case. (d) Front view and side views of the face mask.

of the children's mask must be adjusted and redesigned. After redesigning, the tightness was much higher than the initial. Figure 1d shows the virtual image of the sensor-integrated mask on a male. A screen recording of an iPhone demonstrates the experience of the AR system (supporting video or QR code in Figure 2).

3.2. Structure of the Sensor-Integrated Mask. The structure of the sensor-integrated face mask is shown in Figure 3. There is an inhalation valve (case) to adjust airflow. This design was inspired by animal noses. Many animals have a strong sense of smell, which is generated by chemical molecules in the flow of air in the nostril cavity.[44] A longer airway creates more surface within the snout of an animal and more distance and time for odors and particles to travel, reacting with the odor receptors and chemical sensors, in the nostril cavity. Meanwhile, the longer air path can maintain the temperature of the air entering the body. This also increases the probability that the particles are filtered inside the nose's surface, which may be detected by the smell receptor. Therefore, the size of the intelligent mask was slightly larger than that of the medical masks, creating a longer air path to facilitate filtration and creating a chamber for installing the temperature sensor, the respiratory sensor, and the electronic microcontroller (Figure 3a,b). The temperature sensor was leaned on the cheek, and the respiratory sensor was in front of the nose. When an individual wears the mask, the microcontroller collects body temperature data in the center and wirelessly transfers them to the smartwatch. Although this is designed as a reusable mask, nanoparticle-coated fabrics still need to be changed or disposed of after a certain time. As a result, a square-case structure was designed on the front part of the mask.

Figure 3c shows the structure of a breathing case in which a conductive fabric with a layer of Au@SnO_2 nanoparticles is placed on the front part of the face mask. Air flew from the environment to the mask, so the conductive fabric could absorb PM2.5 or microbes that pass through the mask. This case allows for the replacement of conductive fabrics when they are completely absorbed by microparticles of air pollution or microbes from patients.

Figure 3d shows a photograph of the 3D-printed face mask. The printed mask was made of TPU, a flexible polymer that could fit the faces while adding two traps to it. The face mask is manufactured by fused deposition modeling (FDM), which is a 3D printing process that uses continuous filaments of thermoplastic materials as ink. In this process, the filament was delivered from a large spool through a moving and heated print extruder head and deposited in the growing work. The head of the extruder is moved under computer control to define the printed form.

3.3. Characterization of Au@SnO_2 Core−Shell Nanoparticles. In this work, Au@SnO_2 core@shell nanoparticles were introduced into the conductive fabric. Figure 4 shows the microstructural characteristics and crystallographic structure of the Au@SnO_2 synthesized. The SEM image of Figure 4a first revealed dense staking of the nanoparticle assembly with an average particle diameter of 35.8 nm. The TEM image of Figure 4b further confirmed the core@shell structure for Au@SnO_2, in which the inner region of the high image contrast was composed of Au, while the outer region of the low image contract comprised SnO_2. The size of the Au core was 15.0 ± 1.5 nm, while the thickness of SnO_2 was 10.4 ± 1.6 nm. In Figure 4c, the corresponding XRD pattern further verified the compositions of fcc Au and tetragonal SnO_2 for Au@SnO_2.

3.4. Filtration Efficiency of Modified Conductive Fibers with Nanoparticles. To study the efficiency of filtration, pristine conductive fabric and fabric modified with Au@SnO_2 were tested and compared under nonbiased (0 V) and applied biased conditions (3.3 V). The air from burning incense full of PM2.5 and microparticles flew through the fabric at 0 s. Subsequently, the IR-based PM2.5 sensor was placed on the other side of the fabric to evaluate the filtration efficiency. Comparative results are shown in Figure 4c. The red and blue lines represent the results of a pristine conductive fabric under 0 and 3.3 V. Yellow and green are the results of the use of conductive fabric modified with Au@SnO_2 at 0 and 3.3 V. Several important points can be concluded. First, the application of bias can effectively improve the filtration efficiency of the conductive fabric with respect to PM2.5. This improvement can be attributed to the development of an electric field and static electric charges in the conductive fabric under bias conditions. Second, a significant improvement in filtration efficiency can be achieved by modification with Au@SnO_2 nanoparticles. For Au@SnO_2, the Fermi level equilibrium between Au and SnO_2 would increase the bend on the surface of the SnO_2 shell.[45] This electronic regulation effect could increase the number of positive charges on the surface of SnO_2, further improving the electrostatic interactions between fine particles and the conductive fabric.[46] Therefore, a higher filtration efficiency was obtained. Third, a nearly 100%

https://doi.org/10.1021/acsomega.2c04655
ACS Omega 2022, 7, 42233−42241

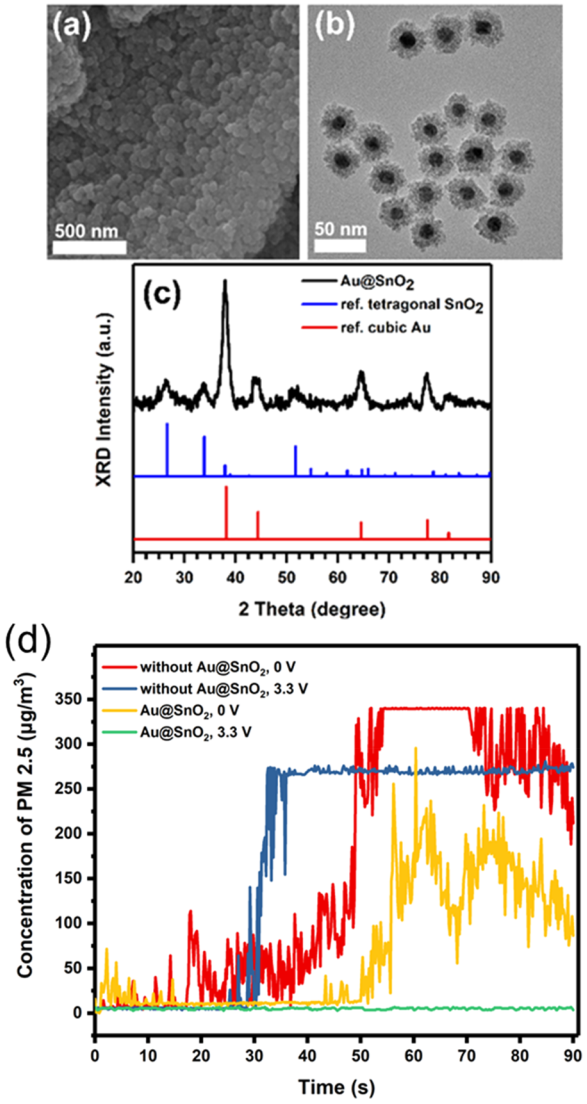

Figure 4. (a) SEM image, (b) TEM image, and (c) corresponding XRD pattern of $Au@SnO_2$ nanoparticles. In (c), the patterns of reference tetragonal SnO2 (JCPDS no. 01-0657) and reference fcc Au (JCPDS no. 01-1172) were also included for comparison. (d) Measurement of the concentration of PM 2.5 concentration ($\mu g/m^3$) using an IR-based sensor after introducing the burning incense air began at 0 s. The lime and green lines represent the results of only using the carbon conductive fiber without $Au@SnO_2$; The dark and light red lines represent the use of the conductive fiber with $Au@SnO_2$.

filtration efficiency could be achieved on conductive fabric modified with $Au@SnO_2$ under 3.3 V. Under bias conditions, the degree of surface band bending in $Au@SnO_2$ could be enhanced. The imparted charges on the fabric and the enhanced surface charge at $Au@SnO_2$ can then cooperate, leading to a greatly improved filtration efficiency.[47]

3.5. Integration of Body Temperature Sensors into the Face Mask. In this investigation, LM35DZ, a thermosensor that could directly measure the temperature on the Celsius scale as a body temperature sensor, was used. The built-in thermal resistance and the inside voltage sensing circuit allowed it to sense between 0 and 100 °C with ±1/4 °C accuracy at room temperature without additional calibration processing. Within the working voltage, the current consumed by the chip was only 50 μA, so we assumed that heat dissipation by this chip could be ignored according to the description of the datasheet. When the user puts on the mask, the temperature sensor should contact the skin of the cheek directly and transmit the body temperature to the microcontroller inside the mask.

3.6. Integration of the Respiratory Rate Sensor into the Face Mask. The respiratory rate is an important indicator of the reflected physical state of the human body. To measure the breathing frequency of the patient or healthcare workers, we used a ceramic piezoelectric patch to detect a change in air pressure. The ceramic piezoelectric patch is a small round patch made of piezoelectric materials that generate voltages when it vibrates. When the force on the piezoelectric materials is applied, their deformation forces the positive and negative ions inside to move around to resist the change, thus creating different electric potentials on the opposite sides of the materials.[48] Its response to force changes sensitively, including the vibration caused by air pressure. Therefore, we put a ceramic piezoelectric patch inside the mask near the nose to convert the vibration signal induced by the respiratory into the respiratory signal of the user.

During the respiratory period, all inhalations and exhalations generated vibration signals, and we collected them by forming a voltage divider circuit between the ceramic piezoelectric patch and the general-purpose input/output (GPIO) of the microcontroller. However, this signal was mixed with noise from user movement. Therefore, signal processing was applied to reveal the actual respiratory signal. The first step was to set up a threshold to filter out some noise that was too small compared to the signal generated by breath. After that, we calculated the first derivation of the signal and deleted the values that were too big, which were caused by the sudden huge vibrations of the sensor. Consequently, the respiratory rate could be calculated with these filtered signals. The flowchart for the measurement of respiratory rate and signal before and after filtering is shown in Figure 5a. The optimization of the respiration rate sensor is in "SI-3 The optimization of the breathing rate sensor".

3.7. Multifunctional Smartwatch. To display physical data and integrate real-time sensors, the smartwatch was designed to pair with the sensor-integrated mask. The smartwatch comprises a microcontroller, a wireless transmission module, a photoplethysmography (PPG) heart rate sensor, and an OLED screen. The smartwatch could display body temperature and the respiratory rate received from the temperature sensor and the respiratory sensor embedded in the face mask through the wireless transmission module (NRF24L01+). These data were encoded and processed through the microcontroller and finally displayed. In addition to the information from the sensors, the OLED screen on the smartwatch allowed the user to check the time and could have customized functions, such as showing a certain picture.

3.8. Heart Rate Sensor on the Multifunctional Smartwatch. The heart rate sensor was manufactured using the Max30102 module for the measurement of PPG on the skin surface, with the advantages of portability, miniaturization, and robustness. PPG provides important information about the human cardiovascular system. In photoplethysmography, when low-intensity infrared (IR) light from light-emitting diodes passes through biological tissues, it is absorbed by bones, skin pigments, venous blood, and arterial blood. Subsequently, the photoreceptor will transfer the photonic signal to the voltage.

https://doi.org/10.1021/acsomega.2c04655
ACS Omega 2022, 7, 42233−42241

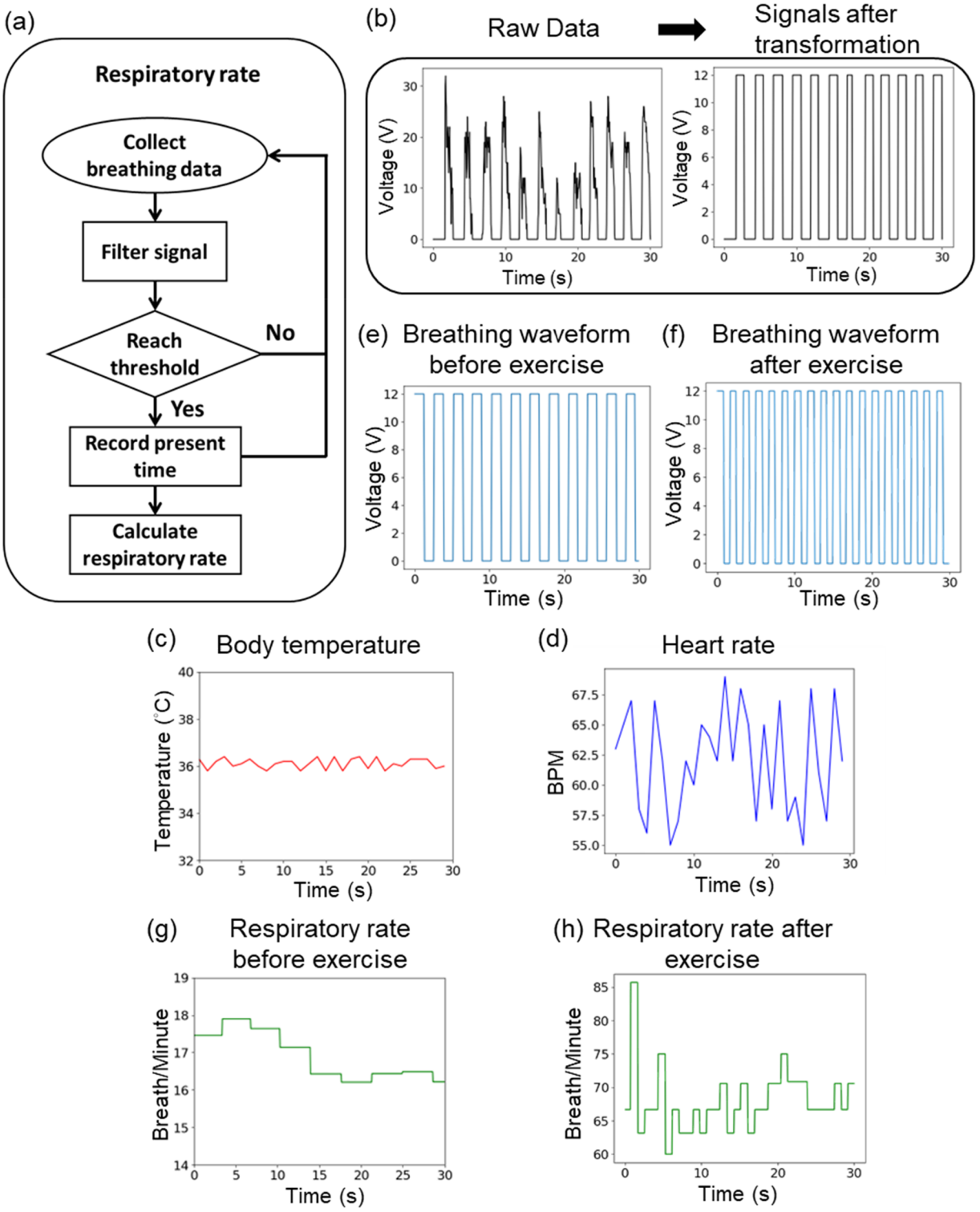

Figure 5. (a) Chart for the flowchart for the calculation of the respiratory rate. (b) Breathing waveform before and after filtering. (c) Body temperature measured by sensor-integrated mask. (d) Heart rate was measured using a sensor-integrated smartwatch. (e,f) Breathing waveform before and after exercise. (g,h) Respiratory rate before and after exercise.

The voltage signal of the PPG is proportional to the amount of blood flow in the blood vessel associated with cardiac activity. Raw signals are sent to a series of filters to remove unwanted frequency components and analyzed with the short-time Fourier transform (STFT).[49−51] Therefore, cardiovascular information could be obtained, including heart rate.

3.9. Sensors and Display on the Smartwatch. Figure 5 shows body temperature, respiratory rate, and heart rate measured by the sensor-integrated face mask and the smartwatch. In Figure 5, the physical state of a person was monitored before and after exercise. Before the exercise, the subject was working in front of a personal computer. His respiratory rate remained within an interval of about 15 to 20

https://doi.org/10.1021/acsomega.2c04655
ACS Omega 2022, 7, 42233−42241

times per minute. However, when the person started exercising, his respiratory rate increased significantly to over 60 times per minute, which was much faster than before exercising. Finally, Figure 6 shows the multifunctional smartwatch.

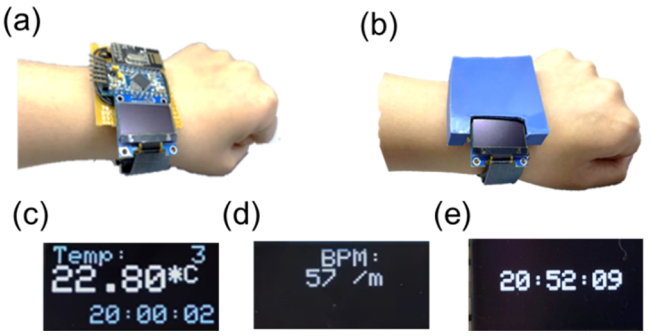

Figure 6. (a) Photograph of the smartwatch and the PPG sensor. (b) Photograph of the smartwatch with a 3D printed case. (c–e) Display panel showing time, heart rate, and temperature.

4. CONCLUSIONS

In conclusion, we develop a wireless temperature and respiratory sensor-integrated face mask based on augmented reality technology and 3D printing. Vital parameters of the human body could be continuously monitored without the need to remove personal protective equipment. Furthermore, a significant improvement in the filtration efficiency of PM 2.5 was also achieved using Au@SnO_2 nanoparticle-modified conductive fibers when an external voltage was applied. A smartwatch with a heart rate sensor was paired with the mask to display sensor data on the mask through wireless transmission. Finally, this sensor-integrated mask system provides the first line of defense to combat global threats from pathogens and air pollutants.

■ ASSOCIATED CONTENT

Supporting Information

The Supporting Information is available free of charge at https://pubs.acs.org/doi/10.1021/acsomega.2c04655.

Augmented reality visualization of masks (MP4)

Additional information as noted in the text, including (SI-1) SEM images of Au@SnO_2 modified conductive fabric, (SI-2) The calibration of the body temperature sensor, (SI-3) The optimization of the breathing rate sensor, (SI-4) Collection of voltage signals caused by respiration, and (SI-5) Eliminating noise from body movement (PDF)

■ AUTHOR INFORMATION

Corresponding Author

Tzu-En Lin − *Institute of Biomedical Engineering, Department of Electrical and Computer Engineering, National Yang Ming Chiao Tung University, 30010 Hsinchu, Taiwan;* orcid.org/0000-0003-4291-3601; Phone: +886 (03) 5731750; Email: telin@nycu.edu.tw

Authors

Ming-Chun Chien − *Institute of Biomedical Engineering, Department of Electrical and Computer Engineering, National Yang Ming Chiao Tung University, 30010 Hsinchu, Taiwan*

Po-Feng Chen − *Institute of Biomedical Engineering, Department of Electrical and Computer Engineering, National Yang Ming Chiao Tung University, 30010 Hsinchu, Taiwan*

Pei-Wen Yang − *Institute of Biomedical Engineering, Department of Electrical and Computer Engineering, National Yang Ming Chiao Tung University, 30010 Hsinchu, Taiwan*

Huai-En Chang − *Department of Material Science, National Yang Ming Chiao Tung University, 30010 Hsinchu, Taiwan*

Ding-Han Wang − *College of Dentistry, National Yang Ming Chiao Tung University, 11221 Taipei, Taiwan*

Tung-Yi Lin − *Institute of Traditional Medicine and Biomedical Industry Ph.D. Program, National Yang Ming Chiao Tung University, Taipei 11221, Taiwan;* orcid.org/0000-0003-1199-1121

Yung-Jung Hsu − *Department of Material Science, National Yang Ming Chiao Tung University, 30010 Hsinchu, Taiwan;* orcid.org/0000-0003-3243-2644

Complete contact information is available at: https://pubs.acs.org/10.1021/acsomega.2c04655

Notes

The authors declare no competing financial interest.

■ ACKNOWLEDGMENTS

T.-E.L. thanks the Young Scholar Fellowship Program of the Ministry of Science and Technology in Taiwan, under Grant MOST 111-2636-E-A49-004, and the Higher Education Sprout Project of the National Yang Ming Chiao Tung University and the Ministry of Education, Taiwan.

■ REFERENCES

(1) Baker, M. A.; Sands, K. E.; Huang, S. S.; Kleinman, K.; Septimus, E. J.; Varma, N.; Blanchard, J.; Poland, R. E.; Coady, M. H.; Yokoe, D. S.; Fraker, S.; Froman, A.; Moody, J.; Goldin, L.; Isaacs, A.; Kleja, K.; Korwek, K. M.; Stelling, J.; Clark, A.; Platt, R.; Perlin, J. B. The Impact of Coronavirus Disease 2019 (COVID-19) on Healthcare-Associated Infections. *Clin. Infect. Dis.* **2022**, *74* (10), 1748−1754.

(2) Haque, M.; Sartelli, M.; McKimm, J.; Bakar, M. A. Health Care-Associated Infections - An Overview. *Infect. Drug Resist.* **2018**, *11*, 2321−2333.

(3) Lazaro, M.; Lazaro, A.; Villarino, R.; Girbau, D. Smart Face Mask with an Integrated Heat Flux Sensor for Fast and Remote People's Healthcare Monitoring. *Sensors* **2021**, *21*, 7472.

(4) Zhong, J.; Li, Z.; Takakuwa, M.; Inoue, D.; Hashizume, D.; Jiang, Z.; Shi, Y.; Ou, L.; Nayeem, O. G.; Umezu, S.; Fukuda, K.; Someya, T.; Zhong, J.; Takakuwa, M.; Inoue, D.; Hashizume, D.; Jiang, Z.; Fukuda, K.; Someya, T.; Li, Z.; Shi, Y.; Ou, L.; Umezu, S.; Nayeem, M. O. G. Smart Face Mask Based on an Ultrathin Pressure Sensor for Wireless Monitoring of Breath Conditions. *Adv. Mater.* **2022**, *34* (6), 2107758.

(5) Lazaro, M.; Lazaro, A.; Villarino, R.; Girbau, D. Smart Mask for Temperature Monitoring with LoRa Backscattering Communication. *2021 6th International Conference on Smart and Sustainable Technologies, SpliTech 2021* 2021, 1−4.

(6) Xia, K.; Li, X.; Li, X.; Liu, Y.; Zhang, H.; Hou, R. Intelligent Anti-epidemic Mask Based on KF and ECF Fusion Algorithm. *Electron. Lett.* **2021**, *57* (19), 724−726.

(7) Zhao, W.; Ma, Y.; Liu, Y. Study on the Design of Intelligent Mask Based on Blood Oxygen Detection Technology. *2021 26th International Conference on Automation and Computing: System*

Intelligence through Automation and Computing, ICAC 2021 2021, 1−6.
(8) Han, S.; Kim, J.; Lee, Y.; Bang, J.; Kim, C. G.; Choi, J.; Min, J.; Ha, I.; Yoon, Y.; Yun, C. H.; Cruz, M.; Wiley, B. J.; Ko, S. H. Transparent Air Filters with Active Thermal Sterilization. *Nano Lett.* **2022**, *22* (1), 524−532.
(9) Yuen, J. G.; Marshilok, A. C.; Todd Benziger, P.; Yan, S.; Cello, J.; Stackhouse, C. A.; Kisslinger, K.; Bock, D. C.; Takeuchi, E. S.; Takeuchi, K. J.; Wang, L.; Babu, S.; Itzkowitz, G.; Thanassi, D.; Knopf, D. A.; Shroyer, K. R. Dry Heat Sterilization as a Method to Recycle N95 Respirator Masks: The Importance of Fit. *PLoS One.* **2022**, *17* (1), No. e0257963.
(10) Shin, J.; Jeong, S.; Kim, J.; Choi, Y. Y.; Choi, J.; Lee, J. G.; Kim, S.; Kim, M.; Rho, Y.; Hong, S.; Choi, J. il; Grigoropoulos, C. P.; Ko, S. H. Dynamic Pore Modulation of Stretchable Electrospun Nanofiber Filter for Adaptive Machine Learned Respiratory Protection. *ACS Nano* **2021**, *15* (10), 15730−15740.
(11) Pan, L.; Wang, C.; Jin, H.; Li, J.; Yang, L.; Zheng, Y.; Wen, Y.; Tan, B. H.; Loh, X. J.; Chen, X. Lab-on-Mask for Remote Respiratory Monitoring. *ACS Mater. Lett.* **2020**, *2* (9), 1178−1181.
(12) Gao, Z.; Lou, Z.; Chen, S.; Li, L.; Jiang, K.; Fu, Z.; Han, W.; Shen, G. Fiber Gas Sensor-Integrated Smart Face Mask for Room-Temperature Distinguishing of Target Gases. *Nano Res.* **2018**, *11* (1), 511−519.
(13) Escobedo, P.; Fernández-Ramos, M. D.; López-Ruiz, N.; Moyano-Rodríguez, O.; Martínez-Olmos, A.; Pérez de Vargas-Sansalvador, I. M.; Carvajal, M. A.; Capitán-Vallvey, L. F.; Palma, A. J. Smart Facemask for Wireless CO2Monitoring. *Nat. Commun.* **2022**, *13* (1), 1−12.
(14) Giovannini, G.; Haick, H.; Garoli, D. Detecting COVID-19 from Breath: A Game Changer for a Big Challenge. *ACS Sens* **2021**, *6* (4), 1408−1417.
(15) Kim, N.; Wei, J. L. J.; Ying, J.; Zhang, H.; Moon, S. K.; Choi, J. A Customized Smart Medical Mask for Healthcare Personnel. In *IEEE International Conference on Industrial Engineering and Engineering Management* 2020, 581−585.
(16) Ramanathan, N.; Chellappa, R. Modeling Age Progression in Young Faces. *Proceedings of the IEEE Computer Society Conference on Computer Vision and Pattern Recognition* 2006, 387−394.
(17) He, R.; Yang, W.; Wu, D.; Wang, H. Age- and Sex-Related Measurements of Total Craniofacial Soft Tissue Thickness and Fat in a Central Chinese Population. *Journal of Craniofacial Surgery* **2021**, *32* (8), 2626−2630.
(18) Zhang, R.; Liu, C.; Hsu, P. C.; Zhang, C.; Liu, N.; Zhang, J.; Lee, H. R.; Lu, Y.; Qiu, Y.; Chu, S.; Cui, Y. Nanofiber Air Filters with High-Temperature Stability for Efficient PM2.5 Removal from the Pollution Sources. *Nano Lett.* **2016**, *16* (6), 3642−3649.
(19) Nguyen, H. T.; Pham, M. T.; Nguyen, T. M. T.; Bui, H. M.; Wang, Y. F.; You, S. J. Modifications of Conventional Organic Membranes with Photocatalysts for Antifouling and Self-Cleaning Properties Applied in Wastewater Filtration and Separation Processes: A Review. *Sep. Sci. Technol.* **2022**, *57*, 1471−1500.
(20) Pillai, O. M.; Sundaramoorthy, S. Development of Photocatalytic Self-Cleaning Textiles Using Tin Oxide and Titanium Dioxide Nanoparticles Mixture. *Journal of The Textile Institute* **2022**, 1−8.
(21) Chen, W.; Feng, X.; Zhang, D.; Lu, F.; Wang, H.; Tan, J.; Xu, Q.; Liu, Y.; Cao, Z.; Su, X. *In Situ* Synthesis of TiO_2 /NC on Cotton Fibers with Antibacterial Properties and Recyclable Photocatalytic Degradation of Dyes. *RSC Adv.* **2022**, *12* (31), 19974−19980.
(22) Tu, W.; Liu, Y.; Chen, M.; Ma, L.; Li, L.; Yang, B. Photocatalytic Self-Cleaning Graphene Oxide Membrane Coupled with Carbon Nitride and Ti3C2-Mxene for Enhanced Wastewater Purification. *Sep. Purif. Technol.* **2022**, *296*, 121398.
(23) Zhang, S.; Hao, J.; Ren, F.; Wu, W.; Xiao, X. Controllable Synthesis of Au@SnO2 Core-Shell Nanohybrids with Enhanced Photocatalytic Activities. *Mater. Res. Express.* **2017**, *4* (5), 055502.
(24) Fu, X.; Li, G. G.; Villarreal, E.; Wang, H. Hot Carriers in Action: Multimodal Photocatalysis on Au@SnO 2 Core-Shell Nanoparticles. *Nanoscale* **2019**, *11* (15), 7324−7334.
(25) Kuo, M. Y.; Hsiao, C. F.; Chiu, Y. H.; Lai, T. H.; Fang, M. J.; Wu, J. Y.; Chen, J. W.; Wu, C. L.; Wei, K. H.; Lin, H. C.; Hsu, Y. J. Au@Cu2O Core@shell Nanocrystals as Dual-Functional Catalysts for Sustainable Environmental Applications. *Appl. Catal., B* **2019**, *242*, 499−506.
(26) Chen, B. D.; Tang, W.; Zhang, C.; Xu, L.; Zhu, L. P.; Yang, L. J.; He, C.; Chen, J.; Liu, L.; Zhou, T.; Wang, Z. L. Au Nanocomposite Enhanced Electret Film for Triboelectric Nanogenerator. *Nano Res.* **2018**, *11* (6), 3096−3105.
(27) Lakkireddy, K.; Kües, U. Bulk Isolation of Basidiospores from Wild Mushrooms by Electrostatic Attraction with Low Risk of Microbial Contaminations. *AMB Express.* **2017**, *7* (1), 1−22.
(28) Hu, J.; Wen, J.; Li, H.; Duan, W.; Fan, S.; Xiao, H.; Chen, S. Experiment and Numerical Simulation on the Fine Particle Migration Behaviors for the Collection Efficiency Enhancement of a Wire-Plate Electrostatic Precipitator in Pig House. *Comput. Electron Agric* **2022**, *199*, 107145.
(29) Gong, Y.; Wang, Y.; Chen, J. Intelligent Anti-Virus Mask Based on Gas Detection Sensor. *J. Phys. Conf. Ser.* **2021**, *1748* (5), 052035.
(30) Frederike Fischer, H.; Wittmann, D.; Baucells Costa, A.; Zhou, B.; Joost, G.; Lukowicz, P. Masquare: A Functional Smart Mask Design for Health Monitoring. *Proceedings - International Symposium on Wearable Computers, ISWC* **2020**, 175−178.
(31) Jung, W.; Lee, J. S.; Han, S.; Ko, S. H.; Kim, T.; Kim, Y. H. An Efficient Reduced Graphene-Oxide Filter for PM 2.5 Removal. *J. Mater. Chem. A. Mater.* **2018**, *6* (35), 16975−16982.
(32) Jeong, S.; Cho, H.; Han, S.; Won, P.; Lee, H.; Hong, S.; Yeo, J.; Kwon, J.; Ko, S. H. High Efficiency, Transparent, Reusable, and Active PM2.5 Filters by Hierarchical Ag Nanowire Percolation Network. *Nano Lett.* **2017**, *17* (7), 4339−4346.
(33) Ghamari, M. A Review on Wearable Photoplethysmography Sensors and Their Potential Future Applications in Health Care. *Int. J. Biosens Bioelectron* **2018**, *4* (4), 195.
(34) Medhi, R.; Li, C. H.; Lee, S. H.; Srinoi, P.; Marquez, M. D.; Robles-Hernandez, F.; Jacobson, A. J.; Lee, T. C.; Lee, T. R. Antimony- And Zinc-Doped Tin Oxide Shells Coated on Gold Nanoparticles and Gold-Silver Nanoshells Having Tunable Extinctions for Sensing and Photonic Applications. *ACS Appl. Nano Mater.* **2020**, *3* (9), 8958−8971.
(35) Xue, Q.; Kan, X.; Pan, Z.; Li, Z.; Pan, W.; Zhou, F.; Duan, X. An Intelligent Face Mask Integrated with High Density Conductive Nanowire Array for Directly Exhaled Coronavirus Aerosols Screening. *Biosens. Bioelectron.* **2021**, *186*, 113286.
(36) Feenstra, B.; Papapostolou, V.; Hasheminassab, S.; Zhang, H.; Boghossian, B. der; Cocker, D.; Polidori, A. Performance Evaluation of Twelve Low-Cost PM2.5 Sensors at an Ambient Air Monitoring Site. *Atmos. Environ.* **2019**, *216*, 116946.
(37) Yang, C. R.; Lin, T. C.; Chang, F. H. Particle Size Distribution and PAH Concentrations of Incense Smoke in a Combustion Chamber. *Environ. Pollut.* **2007**, *145* (2), 606−615.
(38) See, S. W.; Balasubramanian, R. Characterization of Fine Particle Emissions from Incense Burning. *Build Environ* **2011**, *46* (5), 1074−1080.
(39) Chang, Y. C.; Lee, H. W.; Tseng, H. H. The Formation of Incense Smoke. *J. Aerosol. Sci.* **2007**, *38* (1), 39−51.
(40) Jetter, J. J.; Guo, Z.; McBrian, J. A.; Flynn, M. R. Characterization of Emissions from Burning Incense. *Sci. Total Environ.* **2002**, *295* (1−3), 51−67.
(41) Marek Wojciech Sierakowski, K.; Wolinski, T. R.; Domanski, A. W.; Sierakowski, M.; Woliński, T. R.; Domański, A. W.; Osińska, K. *Optical Dust Sensor for the Mining Industry* **2003**, *5064* (1), 122−127.
(42) Babusiak, B.; Smondrk, M.; Borik, S. Design of Ultra-Low-Energy Temperature and Humidity Sensor Based on NRF24 Wireless Technology. *42nd International Conference on Telecommunications and Signal Processing, TSP 2019* 2019, 397−401.
(43) Chen, Q.; Mangadlao, J. D.; Wallat, J.; de Leon, A.; Pokorski, J. K.; Advincula, R. C. 3D Printing Biocompatible Polyurethane/Poly(Lactic Acid)/Graphene Oxide Nanocomposites: Anisotropic Properties. *ACS Appl. Mater. Interfaces.* **2017**, *9* (4), 4015−4023.

https://doi.org/10.1021/acsomega.2c04655
ACS Omega 2022, 7, 42233−42241

(44) Hornung, D. E. Nasal anatomy and the sense of smell. *Taste and Smell* **2006**, *63*, 1−22.
(45) Pan, X.; Zhang, T.; Lu, Q.; Wang, W.; Ye, Z. High Responsivity Ultraviolet Detector Based on Novel SnO2 Nanoarrays. *RSC Adv.* **2019**, *9* (64), 37201−37206.
(46) Gurlo, A. Interplay between O2 and SnO2: Oxygen Ionosorption and Spectroscopic Evidence for Adsorbed Oxygen. *ChemPhysChem* **2006**, *7* (10), 2041−2052.
(47) Xu, J.; Xiao, X.; Zhang, W.; Xu, R.; Kim, S. C.; Cui, Y.; Howard, T. T.; Wu, E. Air-Filtering Masks for Respiratory Protection from PM2.5 and Pandemic Pathogens. *One Earth* **2020**, *3* (5), 574−589.
(48) Kalantarian, H.; Alshurafa, N.; Le, T.; Sarrafzadeh, M. Monitoring Eating Habits Using a Piezoelectric Sensor-Based Necklace. *Comput. Biol. Med.* **2015**, *58*, 46−55.
(49) Boloursaz Mashhadi, M.; Asadi, E.; Eskandari, M.; Kiani, S.; Marvasti, F. Heart Rate Tracking Using Wrist-Type Photoplethysmographic (PPG) Signals during Physical Exercise with Simultaneous Accelerometry. *IEEE Signal Process Lett.* **2016**, *23* (2), 227−231.
(50) Das, S.; Pal, S.; Mitra, M. Real Time Heart Rate Detection from PPG Signal in Noisy Environment. *2016 International Conference on Intelligent Control, Power and Instrumentation, ICICPI 2016* **2017**, 70−73.
(51) Lin, W. H.; Wu, D.; Li, C.; Zhang, H.; Zhang, Y. T. Comparison of Heart Rate Vaiability from PPG with That from ECG. *IFMBE Proc.* **2014**, *42*, 213−2.

https://doi.org/10.1021/acsomega.2c04655
ACS Omega 2022, 7, 42233−42241